Asynchronized Synchronous Motor-Based More Electric Ship – Less Power Electronics for More System Reliability

Kai Ni, *Student Member, IEEE*, Yihua Hu, *Senior Member, IEEE*, Zheng Wang, *Senior Member, IEEE*, Huiqing Wen, *Member, IEEE*, and Chun Gan, *Member, IEEE*

***Abstract*— Nowadays, the fully power decoupled shipboard power system (SPS) architecture is popular. However, the volume of fragile power electronic converters is large, and the system overload capability is low. In this paper, an asynchronized synchronous motor (ASM) based SPS is proposed for more-electric ships (MESs) to handle these issues. The models of simplified synchronous generator (SSG), ASM, back-to-back converter, and supercapacitor bank are established. Besides, the transfer function of SSG excitation system is obtained, with the SSG stability analyzed. Moreover, an ASM control strategy based on emulated stator voltage orientation (ESVO) without phase-locked loop is proposed to control the ASM. By using the proposed ESVO scheme, the impacts on electric machines are mitigated by effective SSG stator power control and ASM torque control. High quality of the three-phase voltage and current waveforms can also be obtained. Furthermore, the simulation study is carried out in Matlab/Simulink to verify the performance of the proposed ASM-SPS. The proposed ESVO scheme and the conventional stator flux oriented control strategy are implemented, and the operation of an induction motor based SPS with grid voltage orientation is also illustrated for comparison, with frequent propulsion load variations taken into consideration.**

***Index Terms*— Asynchronized synchronous motor, shipboard power system, more-electric ship, simplified synchronous generator, emulated stator voltage orientation**

NOMENCLATURE

v, i, ψ	Instantaneous values of voltage, current and flux
R, L, C	Resistance, inductance, and capacitance
L_m, L_{ls}, L_{lr}	Mutual inductance, stator leakage inductance and rotor leakage inductance
L_{ss}, L_s, L_r	Inductances on the source side, stator and rotor ($L_s = L_m + L_{ls}$; $L_r = L_m + L_{lr}$)
σ	Leakage flux factor: $\sigma = 1 - [L_m^2/(L_r L_s)]$
P, Q	Active and reactive power
e	Voltage supply
v_f, v_{f0}	Field voltage, initial field voltage
u	Control signal
S	Switching function
V_{dc}	DC-bus voltage
θ_ψ, θ_s, θ_m	Flux angle, synchronous angle and rotor angle
ω_e, ω_{slip}, ω_r, ω_m	Nominal grid angular frequency, slip angular frequency, and mechanical rotor angular speed
T_e, T_m, T_L	Electromagnetic torque, mechanical/shaft torque, and load torque
n_p, H, k_D	Number of pole pairs, inertia constant, and damping factor
com	Compensating term
k_s	Stator coupling factor
k_a, k_e, k_d	Regulator, exciter and stabilizer gains
t_a, t_e, t_d	Time constants for the regulator, exciter and stabilizer
G, M	Generator and motor
Subscripts & Superscripts	
s, r, ss, t	Stator-side, rotor-side, source-side and terminal values
SG	Variables related to sychronous generator
SC	Variables related to supercapacitors
a, b, c	Phases A, B, C
A, B, C	Points A, B, C
α, β	Direct and quadrature components referred to the stationary reference frame
d, q	Direct and quadrature components referred to the synchrnous reference frame
req, ref, $stab$	Required value; reference value; stablizing value

I. INTRODUCTION

Recently, the increasing shipboard electric power demand accelerates the development of more-electric ships (MESs) [1-3]. The breakthrough in the electrification of marine vessels was achieved by applying power electronic converters in 1990s [4, 5], which gives a sharp rise in the tendency towards DC shipboard power systems (SPSs). There are several advantages for a modern DC SPS: 1) high power efficiency; 2) random speeds for prime movers; 3) fast power generation response time; 4) easy energy storage system (ESS) integration; 5) reduced overall space, cost and weight. Apart from the employment of DC SPS architecture, the integrated power system (IPS) is also gaining popularity [6-9]. For the conventional non-integrated SPS, two subsystems are applied for propulsion and ship service, respectively [10]. By using IPS for MESs, flexible regulation of electrical power among power sources, ESSs, propulsion and service loads can be obtained.

One typical representative that combines the merits of DC

The paper is submitted for review on 03 October 2018.

Kai Ni and Yihua Hu are with the Department of Electrical Engineering & Electronics, University of Liverpool, Liverpool, L69 3GJ, UK (e-mail: k.ni@student.liverpool.ac.uk; y.hu35@liverpool.ac.uk).

Zheng Wang is with the School of Electrical Engineering, Southeast University, Nanjing 210096, China (e-mail: zwang@eee.hku.hk)

Huiqing Wen is with the Department of Electrical & Electronic Engineering, Xi'an Jiaotong-Liverpool University, Jiangsu, China (e-mail: Huiqing.Wen@xjtlu.edu.cn).

Chun Gan is with the School of Electrical and Electronic Engineering, Huazhong University of Science and Technology, Wuhan 430074, China (e-mail: cgan@utk.edu)

SPS and IPS is the medium voltage direct current (MVDC) IPS [11-14]. By employing a large number of power electronic converters, the purposes of on-board space and weight reduction and flexible equipment arrangement are realized, and the system efficiency, survivability and maintainability are improved. However, the challenges of fault detection, location and isolation are presented for MVDC IPS [15-17]. For example, the faulty section has to be completely isolated to ensure the normal operation of the other power components, and the simple "unit-based" protection scheme is no longer feasible [14]. Besides, compared with AC SPS, extremely fast detection and isolation of the faulty sections are required. Since there is a lack of regular zero-crossings in a DC SPS, the arcing faults in DC systems are not likely to extinguish on its own, and enormous fault currents may be caused if the fault isolation is not executed fast enough [18]. By employing solid-state circuit breakers (SSCBs), ultrafast protection speed can be achieved, while high cost and power losses are inevitable. In [19], an optimized SSCB-based DC protection system design was implemented to obtain a compromise of the protection speed and cost. Nevertheless, the coordination of circuit breakers for a selective protection is challenging. Besides, a communication-assisted fault detection method was proposed in [20] to precisely detect the faulty part of the DC network, while the requirement of the control algorithm is high. In order to alleviate the dependence of communication between elements, a fault detection method was put forward in [21] that coordinates the actions of power converters with that of bus contractors, and they only rely on independent local measurements. However, there are a huge number of different scenarios to be considered, and it is difficult to verify that tripping is conducted fast enough for each case.

According to the discussion above, there are still several challenges in developing circuit breaker-based protection methods for DC power systems. Additionally, since the normal operation of MVDC IPS mainly relies on power electronic converters, nonlinear dynamic is induced because of switching behaviors, and the system inertia is greatly reduced, which is detrimental to the system stability [13]. In addition, if the switching frequencies for the power switches are not high enough, the produced current harmonics can seriously affect the power quality. However, if the switching frequencies are too high, the lifetime of power switches can be short, which further shortens the lifetime of MES. The health condition of power electronic converters are difficult to assess, and more power electronic converters will result in more complicated electromagnetic compatibility (EMC) and electromagnetic interference (EMI) problems. Furthermore, many system reliability issues are actually caused by the high failure rate of power electronic converters [22, 23]. In MVDC IPS, full power decoupling is obtained by applying power converters, and power transmission in the system is realized by using DC buses. In this case, the overall system reliability is deteriorated due to the fragility of solid-state devices [22], and additional power losses are encountered. If the normal system operation can still be achieved by employing a reduced volume of power electronic converters, the above mentioned issues can be mitigated. Therefore, a partially power decoupled propulsion system based on an asynchronized synchronous motor (ASM) is proposed in this paper for SPS reliability enhancement and cost saving.

ASM is also named as doubly-fed induction machine (DFIM), which has been widely used in the wind industry due to its small power converter volume. By applying the proposed ASM-SPS for MES, a source-side converter (SSC) and a load-side converter (LSC) are used to regulate the slip power flowing between the rotor of ASM and the stator of synchronous generator (SG). Under this circumstance, the volume of power converters is greatly reduced, and the main part of the generated power is directly fed to the stator of ASM for ship propulsion. In this type of SPS architecture, the power converter interface only deals with partial power flow between the generator and motor. Therefore, there are two power flow paths for the proposed ASM-SPS, as shown in Fig. 1. The main power flow is delivered through motor windings, while the delivery of slip power flow is through power converters in addition to motor windings. Since the metal used for motor windings is much stronger than the solid-state materials used for power converters [24], the main power flow path through motor windings can still keep the shipboard propulsion system work normally even if power converter faults occur. In other words, the breakdown of power converters will not suspend the sailing of MES. Moreover, the mature and cheap AC circuit breakers can be used in the proposed SPS architecture for easy fault protection.

Usually, at least two sets of propulsion systems are required to ensure the normal operation of MES [17], where one of them can function as the auxiliary propulsion system. Since the system reliability is enhanced by using the proposed ASM-SPS, one set of propulsion system is enough for reliable operation, which reduces the cost and system redundancy. Besides, the power distribution for the service loads can still be realized by using DC buses, thus both the advantages of AC and DC SPSs can be obtained. In addition, the speed and torque tracking performance will be evaluated [25, 26]. In the proposed ASM-SPS, the power is supplied by an SG, where a weak grid is formed, in which case the synchronous angle tracking performance of phase-locked loop (PLL) is deteriorated [27]. Therefore, in this paper, a vector control (VC) strategy with

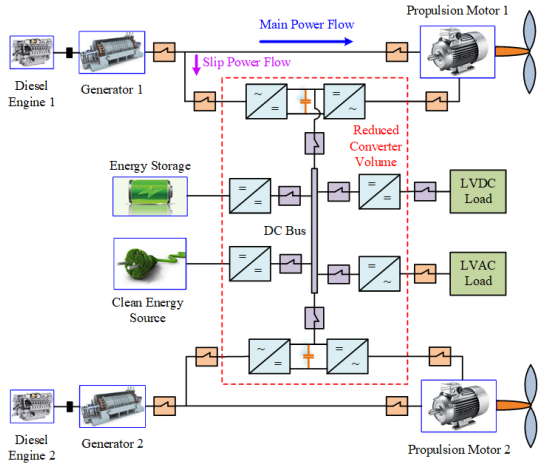

Fig. 1. System configuration of ASM-SPS

emulated stator voltage orientation (ESVO) that does not employ PLL is proposed for ASM-SPS. On top of that, the transfer function of the excitation system of the simplified SG (SSG) is obtained, and its stability is analyzed referring to the changes in the regulator and exciter gains. Moreover, the performance of the proposed ASM-SPS is evaluated for both the cases adopting ESVO and stator flux orientation (SFO) VC schemes. The simulation study for an induction motor (IM) based fully power decoupled SPS with grid voltage oriented (GVO) VC is carried out for comparison. Furthermore, an ESS established by parallel supercapacitors (SCs) and a DC-DC buck/boost converter is presented to eliminate the active power imbalance between the power source and propulsion load during sailing.

The arrangement of this paper is as follows. In Section II, the configuration of the proposed ASM-SPS is illustrated. In Section III, the models of SSG, ASM, back-to-back (BTB) power converter and SC bank are established. Then, the system control scheme is explained in Section IV. Afterwards, the simulation studies are implemented for different SPS architectures and control strategies. Finally, the conclusion is presented in Section VI.

II. System Configuration

In order to reduce the sizes of power electronic converters and increase the reliability of shipboard propulsion system, an ASM-SPS is proposed, which is shown in Fig. 1. Instead of applying a DC distribution line, two paths are used for the ASM to absorb or release power, where the stator of SG is directly connected to that of ASM to supply electric power, while the rotor of ASM is connected to the power source through a BTB power converter. Therefore, only the slip power flows through the BTB power converter. Moreover, the number of DC breakers is decreased compared to a fully power decoupled SPS, which reduces the total cost of protection devices. Furthermore, the breakdown of power converters does not cease the operation of propulsion system, and the back-up propulsion system can be removed for small-scale MESs.

III. Modelling of ASM-SPS

A. SSG

In this paper, an SSG is applied, and the models of diesel engine and drive train are replaced by a speed input. From the system point of view, we regard the SSG as an internal voltage behind an R-L impedance, instead of modelling it in the *dq* rotor reference frame. The saliency of SG is therefore not taken into consideration. Also, the dynamics of the stator, field, and damper windings are neglected, and only the values of internal resistor and inductance are required. Besides, the field voltage of SSG is obtained by a voltage excitation system.

The swing equation of SG is described as

$$\frac{d\omega_{SG}}{dt}=\frac{1}{2H}(T_m-T_{em})-k_D\frac{d\omega_{SG}}{dt} \tag{1}$$

where ω_{SG} is the SG rotor speed; H is the inertia; T_m is the mechanical torque; T_{em} is the electromagnetic torque; and k_D is the damping factor.

The generator type is selected as power-voltage to control the output active power and voltage magnitude. The internal voltage v_f can be derived by excitation, which will be described in the next section.

B. ASM dq Model

With a constant rotor speed, the stator voltage of SSG remains constant, therefore the stator voltage of ASM does not change. By orienting the *d*-axis in the same direction as that of the stator voltage vector, the voltage equations for ASM *dq* model in the synchronous reference frame are derived as

$$\begin{cases}\vec{v}_{sdq}=R_s\vec{i}_{sdq}+\dfrac{d\vec{\psi}_{sdq}}{dt}+j\omega_e\vec{\psi}_{sdq}\\ \vec{v}_{rdq}=R_r\vec{i}_{rdq}+\dfrac{d\vec{\psi}_{rdq}}{dt}+j\omega_{slip}\vec{\psi}_{rdq}\end{cases} \tag{2}$$

where v_{sdq}, v_{rdq} are the stator and rotor *dq* voltages; R_s, R_r are the stator and rotor resistances; i_{sdq}, i_{rdq} are the stator and rotor *dq* currents; ψ_{sdq}, ψ_{rdq} are the stator and rotor *dq* fluxes; ω_e, ω_{slip} are the nominal grid and slip angular speeds.

The stator and rotor flux equations are expressed as

$$\begin{cases}\vec{\psi}_{sdq}=L_s\vec{i}_{sdq}+L_m\vec{i}_{rdq}\\ \vec{\psi}_{rdq}=L_m\vec{i}_{sdq}+L_r\vec{i}_{rdq}\end{cases} \tag{3}$$

where L_s, L_r and L_m are the stator, rotor, and mutual inductances, respectively.

The electromagnetic torque and the kinetic equation of ASM are expressed as

$$T_{em}=1.5n_pL_m(i_{rd}i_{sq}-i_{rq}i_{sd}) \tag{4}$$

$$\frac{d\omega_m}{dt}=\frac{1}{2H}(T_{em}-T_L) \tag{5}$$

where n_p is the number of pole pairs; ω_m is the mechanical rotor angular speed; and T_L is the load torque.

C. BTB Power Converter

There are two power converters in the BTB converter, which are the SSC and LSC. The SSC is directly connected to the AC power transmission line, while the LSC is connected to the rotor of ASM. The topology of BTB converter is displayed in Fig. 2.

The DC-link capacitor is installed to decouple the power regulation of SSC and LSC, and in Fig. 2 the positive direction

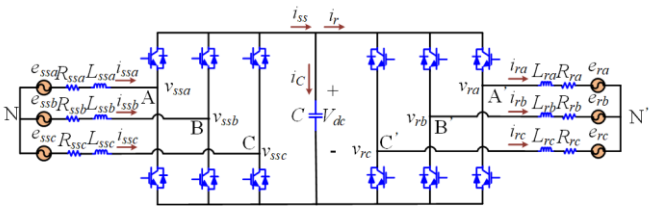

Fig. 2. BTB power converter topology

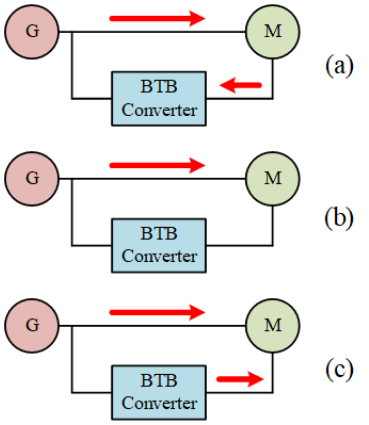

Fig. 3. Operation modes of ASM-SPS (a) Subsynchronous mode; (b) Synchronous mode; (c) Supersynchronous mode

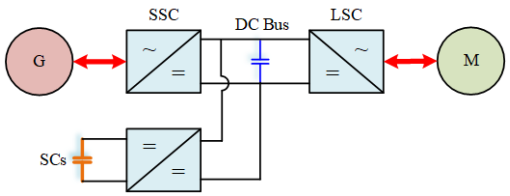

Fig. 4. ESS at the DC bus for ASM-SPS

of power flow is assumed from the SSC to LSC, which caters to the supersynchronous mode. S_{ssa}, S_{ssb} and S_{ssc} are defined as the switching functions of power switches in the three phases of SSC, while S_{la}, S_{lb} and S_{lc} are defined as the switching functions of the power switches in the three phases of LSC. Therefore, the three-phase model of BTB converter can be expressed as

$$\begin{cases} L_{ssx}\dfrac{di_{ssx}}{dt} = e_{ssx} - R_{ssx}i_{ssx} - \dfrac{e_{ssa}+e_{ssb}+e_{ssc}}{3} \\ -[S_{ssx} - \dfrac{S_{ssa}+S_{ssb}+S_{ssc}}{3}]V_{dc}, \qquad x=a,b,c \\ L_{rx}\dfrac{di_{rx}}{dt} = -e_{rx} - R_{rx}i_{rx} + \dfrac{e_{ra}+e_{rb}+e_{rc}}{3} \\ +[S_{lx} - \dfrac{S_{la}+S_{lb}+S_{lc}}{3}]V_{dc}, \qquad x=a,b,c \\ C\dfrac{V_{dc}}{dt} = (S_{ssa}i_{ssa}+S_{ssb}i_{ssb}+S_{ssc}i_{ssc}) - i_r \\ = i_{ss} - (S_{la}i_{ra}+S_{lb}i_{rb}+S_{lc}i_{rc}) \end{cases} \tag{6}$$

$$\begin{cases} v_{ssx} = [S_{ssx} - \dfrac{S_{ssa}+S_{ssb}+S_{ssc}}{3}]V_{dc}, \qquad x=a,b,c \\ v_{rx} = [S_{lx} - \dfrac{S_{la}+S_{lb}+S_{lc}}{3}]V_{dc}, \qquad x=a,b,c \\ i_{ss} = S_{ssa}i_{ssa}+S_{ssb}i_{ssb}+S_{ssc}i_{ssc} \\ i_r = S_{la}i_{ra}+S_{lb}i_{rb}+S_{lc}i_{rc} \end{cases} \tag{7}$$

where L_{ss}, R_{ss}, i_{ss}, v_{ss} and e_{ss} are the source-side inductance, resistance, current, voltage and voltage supply values, respectively; e_r is the rotor-side voltage supply; i_{ss} and i_r are the DC-side currents for the SSC and LSC; C is the DC-link capacitance; and V_{dc} is the DC-bus voltage.

Substituting (7) into (6), the three-phase model can be updated as

$$\begin{cases} L_{ssx}\dfrac{di_{ssx}}{dt} = e_{ssx} - R_{ssx}i_{ssx} - \dfrac{e_{ssa}+e_{ssb}+e_{ssc}}{3} - v_{ssx}, \qquad x=a,b,c \\ L_{rx}\dfrac{di_{rx}}{dt} = -e_{rx} - R_{rx}i_{rx} + \dfrac{e_{ra}+e_{rb}+e_{rc}}{3} + v_{rx}, \qquad x=a,b,c \\ C\dfrac{V_{dc}}{dt} = i_{ss} - i_r \end{cases} \tag{8}$$

Assume that the three phases on both the source and load sides are balanced ($R_{ssa} = R_{ssb} = R_{ssc} = R_{ss}$; $L_{ssa} = L_{ssb} = L_{ssc} = L_{ss}$; $R_{ra} = R_{rb} = R_{rc} = R_r$; $L_{ra} = L_{rb} = L_{rc} = L_r$). The dq model of BTB converter can be expressed as

$$\begin{cases} L_{ss}\dfrac{d\vec{i}_{ssdq}}{dt} = \vec{e}_{ssdq} - R_{ss}\vec{i}_{ssdq} - \vec{v}_{ssdq} - \mathrm{j}\omega_e L_{ss}\vec{i}_{ssdq} \\ L_r\dfrac{d\vec{i}_{rdq}}{dt} = -\vec{e}_{rdq} - R_r\vec{i}_{rdq} + \vec{v}_{rdq} + \mathrm{j}\omega_{slip}L_r\vec{i}_{rdq} \\ C\dfrac{V_{dc}}{dt} = i_{ss} - i_r \end{cases} \tag{9}$$

D. Operation Modes

The BTB power converter is endowed with the feature of bidirectional power flow ability, which enables the ASM-SPS to operate in different modes according to the load demand. Therefore, when the speed of propulsion motor changes within a small range around the synchronous speed, the power balance between the generation and load can be balanced by changing the direction of power flow through the BTB power converter. In total, there are three operation modes: (1) Subsynchronous mode: The power flows through BTB converter from the rotor of ASM. (2) Synchronous mode: There is no power flow through BTB converter. (3) Supersynchronous mode: The power flows through BTB converter to the rotor of ASM. The three operation modes of ASM-SPS are illustrated in Fig. 3, where G and M represent the generator and motor, respectively.

E. SC Bank

During the operation process of an ASM-SPS, the power generation from the SSG is adjusted according to the load demand. When the propulsion load remains at a constant value, the power generation can meet the load demand with the highest efficiency. However, variations in the load torque are inevitable in practical sailing, which may result in instantaneous power imbalance between the power source and propulsion load. Usually, the DC-link capacitance is not large enough to deal with the power imbalance, therefore an additional energy storage device is needed. In this paper, SCs are integrated to the DC bus of the proposed ASM-SPS through a DC-DC converter, as shown in Fig. 4. The SCs are endowed with good transient performance, and they can be accessed at any operation point [28]. More importantly, they assist in regulating the DC-bus voltage to improve the system control performance and enhance the system stability. The ESS established by SC banks functions as either a source or sink to complement the power difference

between the active powers at the source and load sides. The capacitance of the SC is determined by

$$C_{SC} = \frac{2P_n T_{SC}}{V_{SCn}^2} \tag{10}$$

where P_n indicates the rated power of ASM in watts; T_{SC} is the desired time period (in seconds) for the SC bank to exchange energy when ASM operates at the rated power; V_{SCn} is the rated voltage of SC bank in volts.

IV. Control of ASM-SPS

A. Control of SSG

The SSG stator voltage v_{sabc_SG} is regulated by an excitation system to provide the field voltage v_f. In addition to v_{sabc_SG}, a reference voltage v_{ref} (1pu in this paper) and a stabilizing voltage v_{stab} (0 in this paper) are employed. After the regulation, an exciter is applied to generate the field voltage. Moreover, a stabilizer is added to feed the field voltage component back to form a closed loop control architecture. The SSG control block diagram is shown in Fig. 5.

The terminal voltage v_t, which is the magnitude of SSG stator voltage without high order harmonic components, is also applied as a feedback, since it is produced by the magnetic flux induced by the field voltage. In order to conveniently express the transfer function $G(s)$, the input voltage is defined as

$$v_{in} = v_{ref} + \frac{v_{f0}}{k_a} + v_{stab} - v_t \tag{11}$$

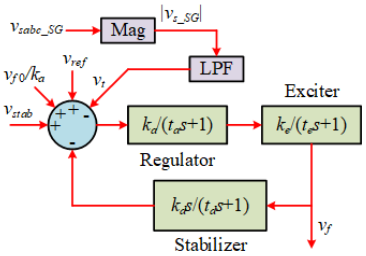

Fig. 5. SSG control block diagram

TABLE I
DETAILS OF THE PARAMETERS IN $G(s)$

Parameters	Values
A	$t_a^2 t_e^2 t_d = 10^{-15}$
B	$t_a t_e(t_a t_e + 2t_a t_d + 2t_e t_d) \approx 2.2\times10^{-11}$
C	$2t_a^2 t_e + 2t_a t_e^2 + 4t_a t_e t_d + t_e^2 t_d + t_a t_e k_a k_e k_d = 10^{-7} k_a k_e k_d + 4.122\times10^{-8}$
D	$(t_a + t_e)^2 + 2(t_a t_e + t_a t_d + t_e t_d) + (t_a + t_e) k_a k_e k_d \approx 1.1\times10^{-3} k_a k_e k_d + 2.1\times10^{-4}$
E	$2t_a + 2t_e + t_d + k_a k_e k_d \approx k_a k_e k_d + 0.1$
X	$t_a t_e t_d k_a k_e = 10^{-8} k_a k_e$
Y	$(t_a t_e + t_a t_d + t_e t_d) k_a k_e \approx 1.1\times10^{-4} k_a k_e$
Z	$(t_a + t_e + t_d) k_a k_e \approx 0.1 k_a k_e$
W	$k_a k_e$

where v_{ref} is the reference voltage; v_{f0} is the initial field voltage; v_{stab} is the stabilizing voltage; v_t is the terminal voltage; and k_a is the regulator gain.

According to Fig. 5, the relationship between v_f and v_{in} can be expressed as

$$v_f = (v_{in} - \frac{k_d s}{t_d s + 1} v_f) \frac{k_a k_e}{(t_a s + 1)(t_e s + 1)} \tag{12}$$

where k_e, k_d are the exciter and stabilizer gains; t_a, t_e and t_d are the regulator, exciter and stabilizer time constants, respectively.

Therefore, the transfer function $G(s)$ can be derived as

$$G(s) = \frac{v_f}{v_{in}} = \frac{Xs^3 + Ys^2 + Zs + W}{As^5 + Bs^4 + Cs^3 + Ds^2 + Es + 1} \tag{13}$$

The time constants have the following values: $t_a = 10^{-3}$s, $t_e = 10^{-4}$s, and $t_d = 0.1$s. The details of A, B, C, D, E, X, Y, Z and W are displayed in TABLE I. As A is too small compared with the other parameters, the s^5 term in the denominator can be ignored, and (13) can be updated as

$$G(s) \approx \frac{10^{-8} k_a k_e s^3 + 1.1\times10^{-4} k_a k_e s^2 + 0.1 k_a k_e s + k_a k_e}{[2.2\times10^{-11} s^4 + (10^{-7} k_a k_e k_d + 4.122\times10^{-8}) s^3 + (1.1\times10^{-3} k_a k_e k_d + 2.1\times10^{-4}) s^2 + (k_a k_e k_d + 0.1) s + 1]} \tag{14}$$

From (14), $G(s)$ can be further modified by setting $K_{ae} = k_a k_e$.

$$G(s) \approx \frac{10^{-8} K_{ae} s^3 + 1.1\times10^{-4} K_{ae} s^2 + 0.1 K_{ae} s + K_{ae}}{[2.2\times10^{-11} s^4 + (10^{-7} K_{ae} k_d + 4.122\times10^{-8}) s^3 + (1.1\times10^{-3} K_{ae} k_d + 2.1\times10^{-4}) s^2 + (K_{ae} k_d + 0.1) s + 1]} \tag{15}$$

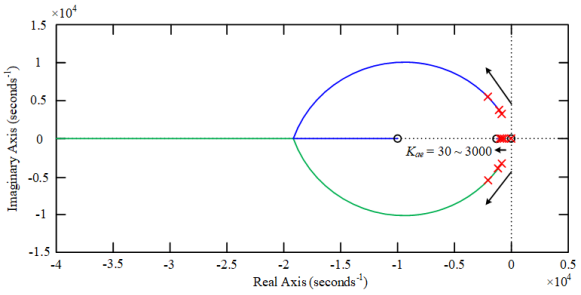

Fig. 6. Root locus of $G(s)$

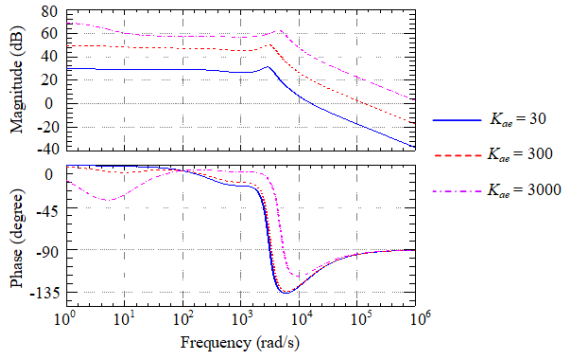

Fig. 7. Magnitude and phase responses of $G(s)$

In this paper, the stabilizer gain k_d is chosen as 10^{-4}, and the effect of change in K_{ae} on the transfer function is investigated. The values of 30, 300 and 3000 are selected for stability analysis. The root locus of $G(s)$ is derived as shown in Fig. 6.

According to the root locus shown in Fig. 6, the system is stable when the value of K_{ae} varies between 30 and 3000. The dominant poles are all on the real axis, with the values between around (-0.1) and 0. The Bode plots of $G(s)$ with different values of K_{ae} are depicted in Fig. 7.

It can be seen from the magnitude response that the magnitude starts to decrease between 10^3rad/s and 10^4rad/s for each case, and it approaches zero at around 10^4rad/s, 10^5rad/s, and 10^6rad/s for K_{ae} = 30, 300 and 3000, respectively. For the phase response, with the increase in K_{ae}, the phase drop in the low frequency region becomes deeper, which negatively affects the generator performance. On the other hand, the phase value is closer to 0 between 10^3rad/s and 10^4rad/s and it recovers to (-90°) faster when K_{ae} is higher. With the overall consideration, 300 is chosen as the value for K_{ae}.

B. *Control of ASM*

The ASM-SPS can be regarded as an islanded microgrid, and the only power source is SSG, thus forming a weak grid. In this case, deteriorated tracking performance for the angle of source-side voltage or stator flux is presented for PLL, and extremely poor small signal stability performance is presented as the load is fully supported by ASM. In this paper, the flux angle θ_ψ is directly estimated, and then 90° is added to it to derive the synchronous angle θ_s. The tracking performance is good enough when the stator resistance is neglected. The control block diagram based on the proposed ESVO-VC for ASM-SPS is displayed in Fig. 8.

The control of SSC and that of LSC are decoupled by the DC-link capacitor on the DC bus. In the SSC control process, the *d*-axis source-side reference current component i_{ssd_ref} is derived by regulating the DC-bus voltage V_{dc}. The SSC control aims to keep V_{dc} stable. In addition, the value of *q*-axis source-side reference current component i_{ssq_ref} is set as 0 to obtain a unity power factor. Besides, the quality of source-side currents is dependent on the current control performance. The *dq* voltage equations at the source side are expressed as

$$\begin{cases} v_{ssd} = v_{sd} - R_{ss}i_{ssd} - L_{ss}\dfrac{di_{ssd}}{dt} + \omega_e L_{ss} i_{ssq} \\ v_{ssq} = v_{sq} - R_{ss}i_{ssq} - L_{ss}\dfrac{di_{ssq}}{dt} - \omega_e L_{ss} i_{ssd} \end{cases} \tag{16}$$

According to (16), the source-side compensating terms *com*1 and *com*2 can be derived as

$$\begin{cases} com1 = -R_{ss}i_{ssd} + \omega_e L_{ss} i_{ssq} \\ com2 = -R_{ss}i_{ssq} - \omega_e L_{ss} i_{ssd} \end{cases} \tag{17}$$

For LSC, the *d*-axis rotor current component i_{rd} is controlled to regulate the electromagnetic torque T_{em}, thus controlling the stator active power P_s and the rotor speed ω_m. On the other hand, the *q*-axis rotor reference current component i_{rq_ref} is achieved by regulating the stator reactive power Q_s, and the control of i_{rq} is related to the control of air-gap field, which ultimately affects the reactive power output. Similar to (16), the rotor-side *dq* voltage equations are obtained as

$$\begin{cases} v_{rd} = R_r i_{rd} + \sigma L_r \dfrac{di_{rd}}{dt} - \omega_{slip}\psi_{rq} \\ v_{rq} = R_r i_{rq} + \sigma L_r \dfrac{di_{rq}}{dt} + \omega_{slip}\psi_{rd} \end{cases} \tag{18}$$

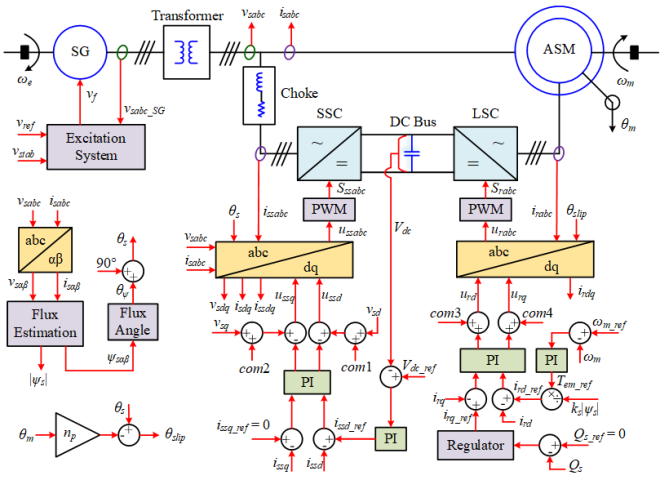

Fig. 8. ESVO-VC for ASM-SPS

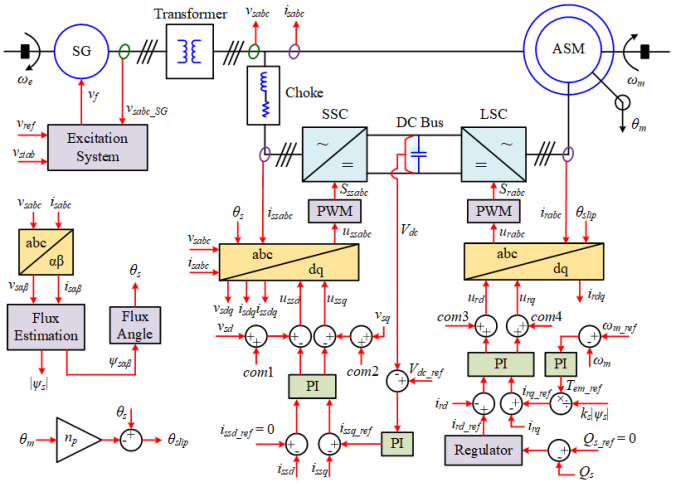

Fig. 9. SFO-VC for ASM-SPS

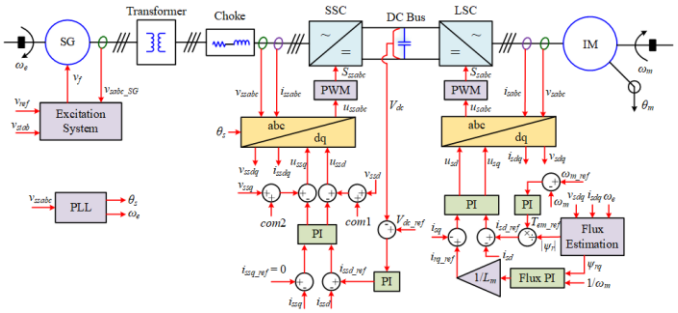

Fig. 10. GVO-VC for IM-SPS

where σ is the leakage flux factor ($\sigma = 1 - [L_m^2/(L_rL_s)]$); ω_{slip} is the slip angular speed, and it is calculated by

$$\omega_{slip} = \omega_e - n_p\omega_m \tag{19}$$

Different from the source side, mutual effects exist between the stator and rotor of ASM, and the expressions of ψ_{rd} and ψ_{rq} are not directly available from the rotor-side parameters and variables. Instead, the mutual components produced by the stator flux should be taken into consideration. When the *d*-axis of synchronous reference frame is in the same direction as that of the stator voltage vector, ψ_{rd} and ψ_{rq} can be obtained as

$$\begin{cases} \psi_{rd} = \sigma L_r i_{rd} \\ \psi_{rq} = -\dfrac{k_s}{\omega_e} + \sigma L_r i_{rq} \end{cases} \tag{20}$$

where $k_s = L_m/L_s$ is the stator coupling factor.

Substitute (20) into (18), the rotor voltage equations can be updated as

$$\begin{cases} v_{rd} = R_r i_{rd} + \sigma L_r \dfrac{di_{rd}}{dt} - \omega_{slip}\left(-\dfrac{k_s}{\omega_e} + \sigma L_r i_{rq}\right) \\ v_{rq} = R_r i_{rq} + \sigma L_r \dfrac{di_{rq}}{dt} + \omega_{slip}\sigma L_r i_{rd} \end{cases} \tag{21}$$

The rotor-side compensating terms *com*3 and *com*4 are

$$\begin{cases} com3 = R_r i_{rd} - \omega_{slip}\left(-\dfrac{k_s}{\omega_e} + \sigma L_r i_{rq}\right) \\ com4 = R_r i_{rq} + \omega_{slip}\sigma L_r i_{rd} \end{cases} \tag{22}$$

Alternatively, the VC of ASM also can be based on SFO. In this case, the orientation of *dq* frame is based on the direction of the stator flux. The control block diagram for ASM-SPS with SFO-VC is displayed in Fig. 9. For the purpose of comparing the control performance of the proposed ASM-SPS and that of a fully power decoupled SPS, the operation of an IM based SPS (IM-SPS) with GVO-VC is also investigated. The LSC is connected to the stator of IM, and the control of it is based on the rotor flux estimation. The corresponding control block diagram is shown in Fig. 10.

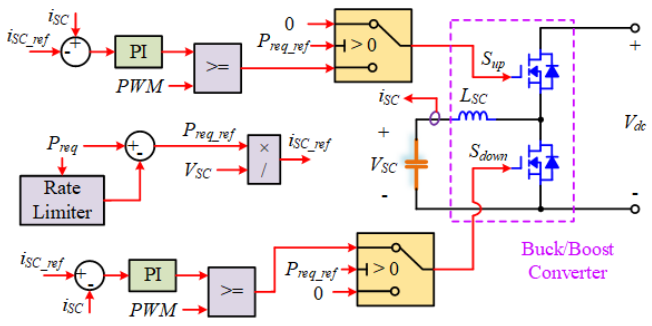

Fig. 11. Control of the buck/boost converter of ESS

C. Control of SC Bank

The SC bank is connected to the DC bus via a DC-DC buck/boost converter. Two power switches are included in the bridge arm of this DC-DC converter, and their duty ratios are controlled separately in the buck and boost operation modes. The operation mode of DC-DC converter and the behaviour of SC bank can be determined according to TABLE II when the ASM operates in different modes.

The positive power flow direction is from SSC to LSC, which corresponds to that in the supersynchronous mode, and the active power required from SC bank is defined as P_{req}.

$$P_{req} = P_r - P_{ss} \tag{23}$$

Then, as the signs of power flows are considered in the calculation process, the determination of the DC-DC converter and SC bank behaviours is not restricted by the operation mode of ASM, and TABLE II can be updated as TABLE III.

In the control process, proportional-integral (PI) controllers

TABLE II
DC-DC CONVERTER AND SC BANK BEHAVIOUR DETERMINATION

ASM	Situation	DC-DC Converter	SC Bank
Subsynchronous	$P_r > P_{ss}$	Boost	Supply Power
	$P_r < P_{ss}$	Buck	Absorb Power
Supersynchronous	$P_r > P_{ss}$	Buck	Absorb Power
	$P_r < P_{ss}$	Boost	Supply Power

TABLE III
UPDATED VERSION OF TABLE II BY INTRODUCING P_{REQ}

P_{req}	DC-DC Converter	SC Bank
> 0	Boost	Supply Power
< 0	Buck	Absorb Power

TABLE IV
PARAMETERS OF SSG

Parameter	Value	Unit
Rated Apparent Power	36	MVA
Rated Frequency	50	Hz
Rated Stator Voltage	13.8	kV
Internal Resistance	0.02	p.u.
Internal Inductance	0.3	p.u.
Inertia Constant	0.35	s
Pole Pairs	20	\

TABLE V
PARAMETERS OF ASM/IM

Parameter	Value	Unit
Rated Apparent Power	36	MVA
Rated Frequency	50	Hz
Rated Stator Voltage	4.16	kV
Stator Resistance	0.023	p.u.
Rotor Resistance	0.016	p.u.
Stator Inductance	0.18	p.u.
Rotor Inductance	0.16	p.u.
Magnetizing Inductance	2.9	p.u.
Friction Factor	0.01	p.u.
Inertia Constant	0.35	s
Pole Pairs	3	\
DC-Link Capacitor	10	mF

are applied for controlling the current through the SC inductor L_{SC}. The pulse width modulation (PWM) signal is produced from a PWM generator. When the converter operates in the buck mode, the duty ratio of the upper switch is controlled to absorb active power. In contrast, when the converter operates in the boost mode, the duty ratio of the lower switch is controlled to supply active power. The control block diagram for the SC bank is shown in Fig. 11.

V. Simulation Results

The operation of the proposed ASM-SPS is verified in Matlab/Simulink2017a. The system operation with the proposed ESVO-VC scheme is compared with that using the traditional SFO-VC strategy. Besides, the performance of an IM-SPS with GVO-VC is illustrated for comparison, and the parameters used for ASM and IM are identical. In the simulation study, the propulsion load variation is taken into consideration (0 ~ 1s: T_L = 1pu; 1 ~ 3s: T_L = 0.8pu; 3 ~ 5s: T_L = 1.2pu). The rotor speed of ASM is controlled at a value around the synchronous angular speed so that the power flowing through the BTB power converter is minimized. The sampling time of simulation is set as 5μs. The parameters used for SSG and ASM/IM are listed in Tables IV & V. The SG stator voltages and currents are displayed in Fig. 12, and the output power is displayed in Fig. 13.

From Fig. 12, it can be seen that the stable operation of SG is achieved by over excitation for all the three scenarios. At 1s, the amplitude of three-phase stator currents drops from 0.5pu to 0.4pu to avoid generating surplus power in the system, while it climbs to 0.6pu instantly after 3s so that the overload requirement is met. In addition, the results indicate that the total harmonic distortions (THDs) in the SG stator voltages and currents are the lowest when applying the proposed ESVO-VC scheme for ASM-SPS.

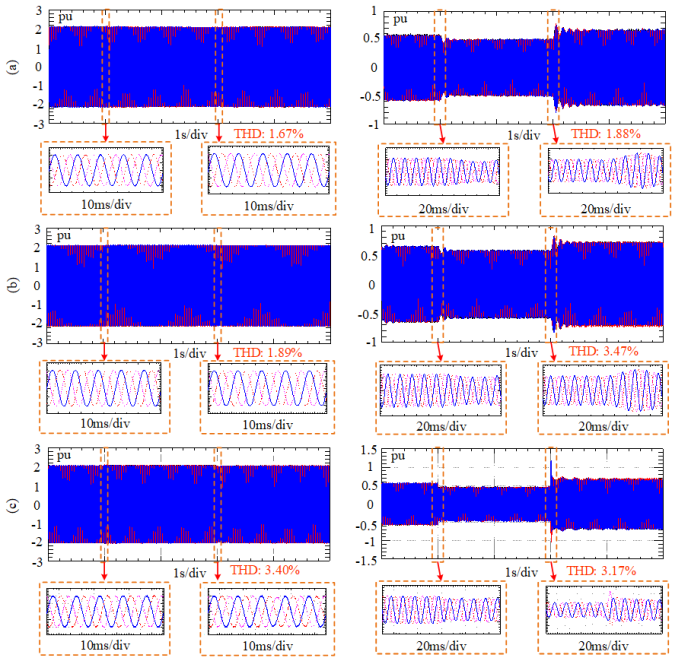

Fig. 12. SG stator voltages (left) and currents (right) for (a) ASM-SPS with ESVO-VC; (b) ASM-SPS with SFO-VC; (c) IM-SPS with GVO-VC

The change in the generated power from the SG follows the load variation for each case, as can be seen in Fig. 13. At the instants of load variations, obvious fluctuations are observed, where the lowest value is smaller than 24MW at around 1s and the largest one exceeds 54MW at around 3s for Figs. 13(a) and (b). It can be seen that there are more fluctuations when the traditional SFO-VC scheme is used, compared with the ESVO-VC case. A large spike in the generated power can be seen in Fig. 13(c) at the instant of load drop.

The performance of SSC is verified by illustrating the stator and SSC three-phase AC currents and the DC-bus voltage for the ASM cases. For the fully power decoupled IM-SPS, the stator currents are directly related to the performance of the shipboard propulsion load. The corresponding waveforms are displayed in Figs. 14 and 15 for the three cases.

From Fig. 14, when the proposed ESVO-VC is applied, the ASM stator-side three-phase currents (THD: 1.68%) have better waveform quality than those in the SFO-VC case (THD: 4.09%). It can be seen that the three-phase currents through SSC are not well regulated by using the traditional SFO-VC, in which the THD reaches 606.67%. On the other hand, almost sinusoidal three-phase source-side current waveforms (THD: 8.90%) are derived by applying the proposed ESVO-VC.

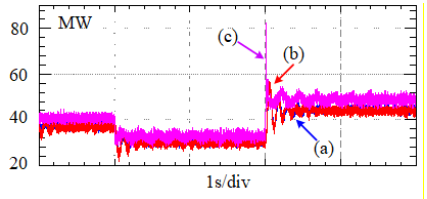

Fig. 13. SG power generation for (a) ASM-SPS with ESVO-VC; (b) ASM-SPS with SFO-VC; (c) IM-SPS with GVO-VC

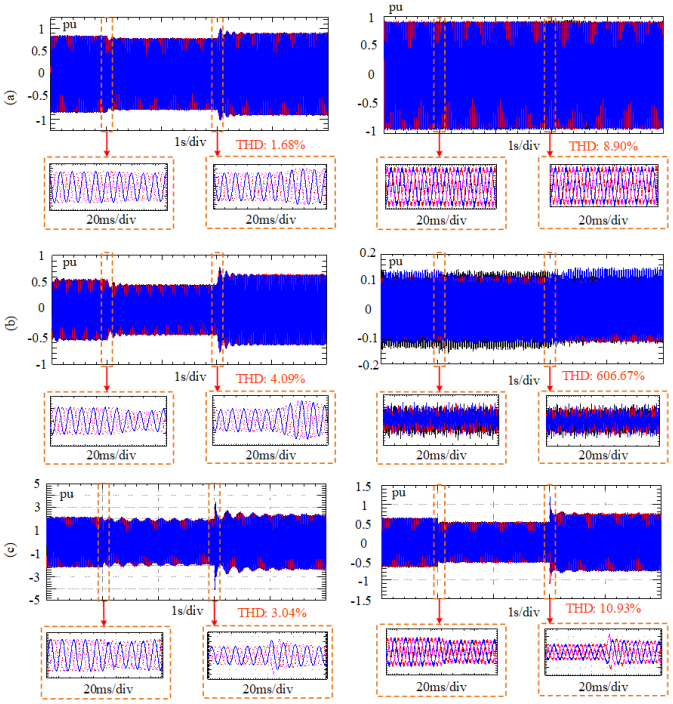

Fig. 14. The stator currents (left) and SSC currents (right) for (a) ASM-SPS with ESVO-VC; (b) ASM-SPS with SFO-VC; (c) IM-SPS with GVO-VC

From Fig. 15, the DC-bus voltage is adjusted to either store or release the active power difference between the power source and load to keep the stable system operation in the ESVO-VC case, although a higher DC-bus voltage level is presented. However, when applying the SFO-VC, the regulation of slip power is not effective, as the DC-link capacitor voltage does not respond to the variations in load torque. In addition, there are obvious transients during the instants of step change in the load torque for the case of IM-SPS with GVO-VC.

The active and reactive powers delivered to the power loads are illustrated in Fig. 16 for the three cases, and the corresponding power factors are shown in Fig. 17.

From Fig. 18, the active power supplied to ASM is almost identical to the power generated by SG for each scenario. However, the magnitude of reactive power for the IM-SPS is much larger than those in the other two cases, and there are significant fluctuations. The phenomenon is clearly reflected in the power factor, which is displayed in Fig. 17, indicating that the lowest value reaches 0.94 for the IM-SPS. There is almost no difference between the power factors for the two control schemes for ASM-SPS, which are both approximately unity.

It can be seen from Fig. 18 that the rotor speed of ASM is approximately kept at a constant value when the load torque is not changing, while some fluctuations are observed at the instants of load variations for the ESVO and SFO-VC schemes for ASM-SPS. In addition, the speed control performance for the IM-SPS is the best among the three cases. Furthermore, according to Fig. 19, the electromagnetic torque precisely tracks the load torque, and the fluctuation is within ± 0.1pu when T_L is stable for the ESVO-VC case, which is almost identical to the situation shown in Fig. 19(c). Nevertheless, more torque fluctuations are presented when applying SFO-VC.

According to the simulation results, effective slip power control can be obtained by using the proposed ESVO-VC scheme, and better system performance in terms of the SG stator power control and ASM torque control is obtained to mitigate the impacts to electrical machines. On top of that, the quality of three-phase voltage and current waveforms by applying the proposed ESVO-VC scheme is higher than that by using the traditional SFO-VC one.

Furthermore, in order to complement the active power required by the load side, 50 SCs with the capacitance of 50F and rated voltage of 6.8kV are connected in parallel to function as the ESS. The initial state of charge (SOC) for each SC is around 49.4%. With the aforementioned propulsion load profile (0 ~ 1s: T_L = 1pu; 1 ~ 3s: T_L = 0.8pu; 3 ~ 5s: T_L = 1.2pu), the active power required from the propulsion load and that supplied from the SC bank are shown in Fig. 20, and the SOC of the SC bank is displayed in Fig. 21. The proposed ESVO-VC scheme is applied in this case.

It can be seen that the active power supplied from energy storage can complement that required by the load, and at the same time, the SOC keeps decreasing, indicating the discharge process of SC bank.

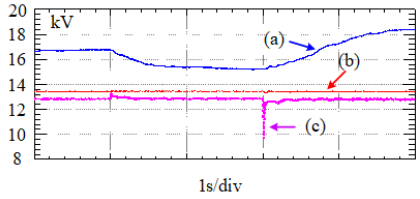

Fig. 15. The DC-bus voltage for (a) ASM-SPS with ESVO-VC; (b) ASM-SPS with SFO-VC; (c) IM-SPS with GVO-VC

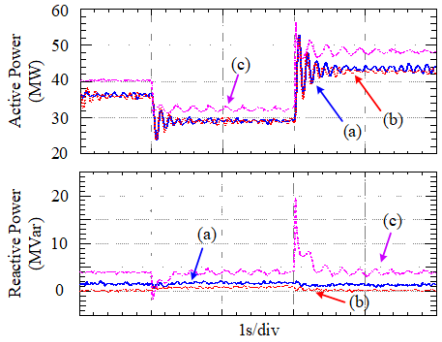

Fig. 16. Active and reactive powers for (a) ASM-SPS with ESVO-VC; (b) ASM-SPS with SFO-VC; (c) IM-SPS with GVO-VC

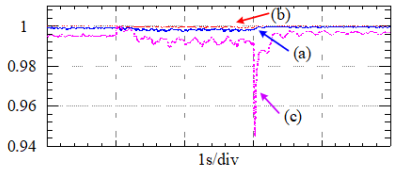

Fig. 17. Power factor for (a) ASM-SPS with ESVO-VC; (b) ASM-SPS with SFO-VC; (c) IM-SPS with GVO-VC

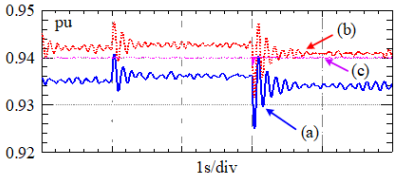

Fig. 18. Rotor speed for (a) ASM-SPS with ESVO-VC; (b) ASM-SPS with SFO-VC; (c) IM-SPS with GVO-VC

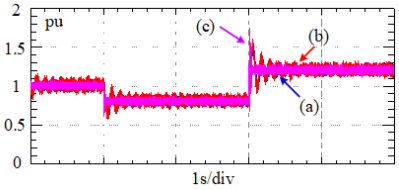

Fig. 19. Electromagnetic torque for (a) ASM-SPS with ESVO-VC; (b) ASM-SPS with SFO-VC; (c) IM-SPS with GVO-VC

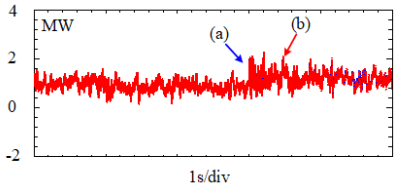

Fig. 20. The active power (a) required by the propulsion load (blue solid line); (b) supplied by the SC bank (read dash line)

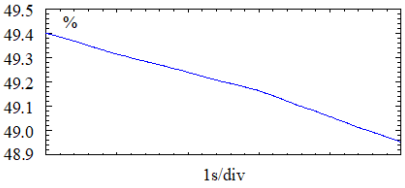

Fig. 21. SOC of SC bank

VI. Conclusion

An ASM-SPS is proposed in this paper to enhance the system reliability by depriving the dominating position of power electronics in MVDC IPS. The models of SSG, ASM, BTB converter, and SC bank are established. In addition, the transfer function of the SSG excitation system is derived, and the root locus and bode diagrams are analyzed. Moreover, the ESVO-VC strategy without using PLL is illustrated to control the ASM in the working condition with a nearly synchronous speed. The impacts on semiconductor switches are maximally mitigated during load change. Moreover, a high power factor is derived, and the electromagnetic torque precisely tracks the load torque. Furthermore, the implementation of SC bank as the ESS complements the power insufficiency at the propulsion load.

The ASM-SPS performance is evaluated in the simulation study by comparing the cases by using the proposed ESVO-VC and the traditional SFO-VC, and the operation of IM-SPS is also illustrated. The following points can be obtained.

1) Effective slip power regulation can be obtained by using the proposed ESVO-VC.

2) Better SSG stator power control and ASM torque control are derived in the ESVO-VC case, thus mitigating the impacts to the on-board electric machines.

3) The three-phase voltage and current waveforms achieved by employing the ESVO-VC have the highest quality.

4) The speed control performance is good enough for the investigated working condition.

Overall, by applying the proposed ESVO-VC for ASM-SPS, cost effective shipboard energy management is obtained with enhanced system reliability even if frequent load variations are presented.

References

[1] J. F. Hansen and F. Wendt, "History and State of the Art in Commercial Electric Ship Propulsion, Integrated Power Systems, and Future Trends," *Proceedings of the IEEE*, vol. 103, no. 12, pp. 2229-2242, Nov. 2015.

[2] A. Vicenzutti, D. Bosich, G. Giadrossi, and G. Sulligoi, "The Role of Voltage Controls in Modern All-Electric Ships: Toward the all electric ship," *IEEE Electr. Mag.*, vol. 3, no. 2, pp. 49-65, May 2015.

[3] E. Skjong, E. Rodskar, M. Molinas, T. A. Johansen, and J. Cunningham, "The Marine Vessel's Electrical Power System: From its Birth to Present Day," *Proceedings of the IEEE*, vol. 103, no. 12, pp. 2410-2424, Dec. 2015.

[4] *IEEE recommended practice for 1 to 35kV medium voltage DC power systems on ships.*, 2010.

[5] Z. Jin, L. Meng, J. M. Guerrero, and R. Han, "Hierarchical Control Design for a Shipboard Power System With DC Distribution and Energy Storage Aboard Future More-Electric Ships," *IEEE Trans. Ind. Informat.*, vol. 14, no. 2, pp. 703-714, Feb. 2018.

[6] G. Seenumani, J. Sun, and H. Peng, "Real-Time Power Management of Integrated Power Systems in All Electric Ships Leveraging Multi Time Scale Property," *IEEE Trans. Control Syst.Technol.*, vol. 20, no. 1, pp. 232-240, Jan. 2012.

[7] T. J. McCoy, "Integrated power systems—An outline of requirements and functionalities for ships," *Proceedings of the IEEE*, vol. 103, no. 12, pp. 2276-2284, Nov. 2015.

[8] G. Sulligoi, A. Vicenzutti, and R. Menis, "All-Electric Ship Design: From Electrical Propulsion to Integrated Electrical and Electronic Power Systems," *IEEE Trans. Transport. Electr.*, vol. 2, no. 4, pp. 507-521, Dec. 2016.

[9] F. D. Kanellos, A. Anvari-Moghaddam, and J. M. Guerrero, "A cost-effective and emission-aware power management system for ships with integrated full electric propulsion," *Electric Power Systems Research*, vol. 150, pp. 63-75, May 2017.

[10] S.-Y. Kim, S. Choe, S. Ko, and S.-K. Sul, "A Naval Integrated Power System with a Battery Energy Storage System: Fuel efficiency, reliability, and quality of power," *IEEE Electr. Mag.*, vol. 3, no. 2, pp. 22-33, Jun. 2015.

[11] G. Sulligoi, A. Tessarolo, V. Benucci, M. Baret, A. Rebora, and A. Taffone, "Modeling, Simulation, and Experimental Validation of a Generation System for Medium-Voltage DC Integrated Power Systems," *IEEE Trans. Ind. Appl.*, vol. 46, no. 4, pp. 1304-1310, Jul./Aug. 2010.

[12] M. Cupelli *et al.*, "Power Flow Control and Network Stability in an All-Electric Ship," *Proceedings of the IEEE*, vol. 103, no. 12, pp. 2355-2380, Nov. 2015.

[13] A. Riccobono *et al.*, "Stability of Shipboard DC Power Distribution: Online Impedance-Based Systems Methods," *IEEE Electr. Mag.*, vol. 5, no. 3, pp. 55-67, Sep. 2017.

[14] R. M. Cuzner and V. Singh, "Future Shipboard MVdc System Protection Requirements and Solid-State Protective Device Topological Tradeoffs," *IEEE J. Emerg. Sel. Topics Power Electron.*, vol. 5, no. 1, pp. 244-259, Mar. 2017.

[15] M. Saeedifard, M. Graovac, R. F. Dias, and R. Iravani, "DC Power Systems: Challenges and Opportunities," presented at the IEEE PES General Meeting, Providence, RI, USA, Jul., 2010.

[16] M. Babaei, J. Shi, and S. Abdelwahed, "A Survey on Fault Detection, Isolation, and Reconfiguration Methods in Electric Ship Power Systems," *IEEE Access*, vol. 6, pp. 9430-9441, Mar. 2018.

[17] K. Satpathi, A. Ukil, and J. Pou, "Short-Circuit Fault Management in DC Electric Ship Propulsion System: Protection Requirements, Review of Existing Technologies and Future Research Trends," *IEEE Trans. Transport. Electr.*, vol. 4, no. 1, pp. 272-291, Mar. 2018.

[18] A. A. S. Emhemed, K. Fong, S. Fletcher, and G. M. Burt, "Validation of Fast and Selective Protection Scheme for an LVDC Distribution Network," *IEEE Trans. Power Del.*, vol. 32, no. 3, pp. 1432-1440, Jun. 2017.

[19] L. L. Qi, A. Antoniazzi, L. Raciti, and D. Leoni, "Design of Solid-State Circuit Breaker-Based Protection for DC Shipboard Power Systems," *IEEE J. Emerg. Sel. Topics Power Electron.*, vol. 5, no. 1, pp. 260-268, Mar. 2017.

[20] M. Monadi, C. Gavriluta, A. Luna, J. I. Candela, and P. Rodriguez, "Centralized Protection Strategy for Medium Voltage DC Microgrids," *IEEE Trans. Power Del.*, vol. 32, no. 1, pp. 430-440, Feb. 2017.

[21] P. Cairoli and R. A. Dougal, "Fault Detection and Isolation in Medium-Voltage DC Microgrids: Coordination Between Supply Power Converters and Bus Contactors," *IEEE Trans. Power Electron.*, vol. 33, no. 5, pp. 4535-4546, May 2018.

[22] S. Yang, A. Bryant, P. Mawby, D. Xiang, L. Ran, and P. Tavner, "An Industry-Based Survey of Reliability in Power Electronic Converters," *IEEE Trans. Ind. Appl.*, vol. 47, no. 3, pp. 1441-1451, May/Jun. 2011.

[23] J. Lu, Y. Hu, X. Zhang, Z. Wang, J. Liu, and C. Gan, "High-Frequency Voltage Injection Sensorless Control Technique for IPMSMs Fed by a Three-Phase Four-Switch Inverter With a Single Current Sensor," *IEEE/ASME Trans. Mechatronics*, vol. 23, no. 2, pp. 758-768, Apr. 2018.

[24] J. R. Davis, "Introduction," in *ASM Speciality Handbook: Heat-Resistant Materials*Geauga County, Ohio: ASM International, 1997, pp. 3-67.

[25] Y. Liu, X. Zhu, H. Zhang, and M. Basin, "Improved Robust Speed Tracking Controller Design for an Integrated Motor-Transmission Powertrain System Over Controller Area Network," *IEEE/ASME Trans. Mechatronics*, vol. 23, no. 3, pp. 1404-1414, Jun. 2018.

[26] K. Li, F.-C. Chou, and J.-Y. Yen, "Real-Time, Energy-Efficient Traction Allocation Strategy for the Compound Electric Propulsion System," *IEEE/ASME Trans. Mechatronics*, vol. 22, no. 3, pp. 1371-1380, Jun. 2017.

[27] L. Huang, H. Xin, L. Zhang, Z. Wang, K. Wu, and H. Wang, "Synchronization and Frequency Regulation of DFIG-Based Wind Turbine Generators With Synchronized Control," *IEEE Trans. Energy Convers.*, vol. 32, no. 3, pp. 1251-1262, Sep. 2017.

[28] C. Abbey and G. Joos, "Supercapacitor Energy Storage for Wind Energy Applications," *IEEE Trans. Ind. Appl.*, vol. 43, no. 3, pp. 769-776, May/Jun. 2007.

Kai Ni (S'17) was born in Jiangsu, China. He received the B.Eng. (Hons) degree in Electrical Engineering and Automation from Xi'an Jiaotong Liverpool University, Suzhou, China, and Electrical Engineering from University of Liverpool, Liverpool, UK, in 2016. He is currently pursuing the Ph.D. degree at the University of Liverpool. His research interests include operation and control of doubly-fed induction machines, power electronic converters, and power systems.

Yihua Hu (M'13-SM'15) received the B.S. degree in electrical engineering in 2003, and the Ph.D. degree in power electronics and drives in 2011, both at China University of Mining and Technology. Between 2011 and 2013, he was with the College of Electrical Engineering, Zhejiang University as a Postdoctoral Fellow. Between 2013 and 2015, he worked as a Research Associate at the power electronics and motor drive group, the University of Strathclyde. Currently, he is a Lecturer at the Department of Electrical Engineering and Electronics, University of Liverpool (UoL). He has published 85 papers in IEEE Transactions journals. His research interests include renewable generation, power electronics converters & control, electric vehicle, more electric ship/aircraft, smart energy system and non-destructive test technology. He is the associate editor of *IEEE Transactions on Industrial Electronics*, *IET Renewable Power Generation*, *IET Intelligent Transport Systems* and *Power Electronics and Drives*.

Zheng Wang (S'05–M'09-SM'14) received the B.Eng. and M.Eng. degrees from Southeast University, Nanjing, China, in 2000 and 2003, respectively, and the Ph.D. degree from The University of Hong Kong, Hong Kong, in 2008, all in electrical engineering. From 2008 to 2009, he was a Postdoctoral Fellow in Ryerson University, Toronto, ON, Canada. He is currently a full Professor in the School of Electrical Engineering, Southeast University, China. His research interests include electric drives, power electronics, and distributed generation. He has authored or coauthored over 80 internationally refereed papers and four books in these areas.

Prof. Wang received several academic awards including IEEE PES Chapter Outstanding Engineer Award, Best Paper Award of International Conference on Electrical Machines and Systems (ICMES), Best Session Paper Award of IEEE Annual Meeting of Industrial Electronics (IECON), and Nanjing Outstanding Paper Award of Natural Science.

Huiqing Wen (M'13-SM'18) received his B.S. and M.S. degrees in Electrical Engineering from Zhejiang University, Hangzhou, China, in 2002 and 2006, respectively; and his Ph.D. degree in Electrical Engineering from the Chinese Academy of Sciences, Beijing, China, in 2009. From 2009 to 2010, he was an Electrical Engineer working in the Research and Development Center, GE (China) Co., Ltd., Shanghai, China. From 2010 to 2011, he was an Engineer at the China Coal Research Institute, Beijing, China. From 2011 to 2012, he was a Postdoctoral Fellow at the Masdar Institute of Science and Technology, Abu Dhabi, United Arab Emirates. He is presently working as an Associate Professor at the Xi'an Jiaotong-Liverpool University, Suzhou, China. His current research interests include bidirectional DC-DC converters, power electronics in flexible AC transmission applications, electrical vehicles, and high-power, three-level electrical driving systems.

Chun Gan (M'14) received the Ph.D. degree in electrical engineering and motor drives from Zhejiang University, Hangzhou, China, in 2016.

He is currently a Professor with the School of Electrical and Electronic Engineering, Huazhong University of Science and Technology, Wuhan, China. From 2016 to 2018, he was a Research Associate with the Department of Electrical Engineering and Computer Science, University of Tennessee, Knoxville, TN, USA. He has authored/coauthored more than 80 peer-reviewed technical papers, including more than 40 IEEE Transaction papers. He has fifteen issued/published invention patents. His research interests include electrical motor drives, electrical motor design, electric vehicles, hybrid vehicles, and high-efficiency power converters.

Dr. Gan was the recipient of the 2018 Highlighted Paper Award from IEEE TPEL; the 2018 Marie Sklodowska-Curie Actions Seal of Excellence Award from European Commission; the 2016 Excellent Ph.D. Graduate Award and the 2015 Top Ten Excellent Scholar Award in Zhejiang University.